Innovative Infrastructure Solutions (2024) 9:123
https://doi.org/10.1007/s41062-024-01442-4

TECHNICAL PAPER

Influence of deteriorated stirrups on the shear performance of RC beams incorporating fly ash and enhanced with carbon fiber-reinforced polymer strengthening

Sandeep Sathe[1] · **Sudhir Patil**[1]

Received: 6 January 2024 / Accepted: 12 March 2024 / Published online: 31 March 2024

Abstract
This study presents findings on the impact of corrosion of stirrups on the shear performance of reinforced concrete (RC) beams incorporating fly ash (FA) and strengthened with carbon fiber-reinforced polymer (CFRP). The study has identified that the optimal replacement proportion of cement with FA is 20%, resulting in improved compressive strength and split tensile strength of the concrete. The stirrups of the RC beam were subjected to controlled exposure periods of 4, 8, and 10 days, achieving targeted mass losses of 5%, 10%, and 15%, respectively by the accelerated corrosion method. The CFRP strengthening significantly improved the shear capacity of the RC beams by 9.1% to 23.1% in comparison to the control *RC* beam without corrosion. In the corroded beams, CFRP sheets hindered the development and spread of diagonal cracks, postponing the appearance of critical failures. Failure in the specimens initiated with the debonding of the CFRP from the concrete substrate. This subsequently led to the crushing of the concrete, preventing the CFRP from achieving its ultimate strength capacity. Interestingly, CFRP strengthening was proportionally more effective for corroded RC beams at the same corrosion level. The strengthened corroded beam displayed 20% greater deflection at mid-span than the strengthened uncorroded beam. Applying the proposed equation to the beam yielded a calculated shear capacity in close agreement with the experimental findings.

Keywords Corroded stirrups · Carbon fiber-reinforced polymer · Shear capacity · Corrosion level · Mid-span deflection

Introduction

Many RC structures in corrosive environments are experiencing severe premature deterioration, with signs already appearing in concrete structures built in recent decades. This deterioration caused by steel reinforcement corrosion, poses a threat to structural integrity and safety. Evaluating the performance of corroded RC beams is crucial for assessing durability and conducting necessary maintenance [1–6]. The RC structures face significant safety and durability challenges due to adverse conditions such as marine and industrial environments, increased concentrations of carbon dioxide (CO_2), environmental pollution, acid rain, and the use of improper construction methods [7, 8]. Enhancing the durability of RC structures involves safeguarding the reinforcement from corrosion through the inclusion of admixtures in concrete. Additionally, the maintenance of aging RC structures can be accomplished through the retrofitting of these structures. Corrosion-inhibiting admixtures, such as organic compounds like amines and amides [9–12] and inorganic like Sodium Nitrate, Calcium Nitrite, Zinc Phosphate, and Sodium Silicate slow down the corrosion process by creating a passive layer on the surface of steel reinforcement [13, 14]. Environmentally sustainable corrosion inhibitors, including FA, ground granulated blast-furnace slag, silica fume, and other pozzolanic materials, alter concrete characteristics and enhance the corrosion resistance of the steel reinforcement embedded within the concrete [15–19]. The concrete beams with FA showed better resistance to corrosion compared to conventional concrete beams. While conventional beams lost 72% of their load-carrying capacity after 20% steel weight loss due to corrosion, fly

✉ Sandeep Sathe
sandeepsatheresearch@gmail.com

Sudhir Patil
sudhir.patil@mitwpu.edu.in

[1] School of Civil Engineering, Dr. Vishwanath Karad MIT World Peace University, Pune, Maharashtra 411038, India

ash beams only experienced a 60% reduction [4–6, 20]. The concrete with higher FA content shows improved resistance to accelerated corrosion. Additionally, these corroded FA beams experience larger deflections compared to control samples without FA, indicating a higher level of ductility in the FA beams [4, 5]. The FA in concrete reacts with calcium hydroxide ($Ca(OH)_2$) in the presence of water, forming a C-S–H gel. This gel fills the tiny pores in the concrete, reducing its permeability and enhancing its corrosion resistance [21, 22]. The green concrete boasting enhanced strength and durability was attained through a combination of FA, nanoparticles, and a corrosion inhibitor. [23, 24]

Various retrofitting options exist for enhancing existing RC structures, with bonding thin steel plates being a commonly employed method [25–27]. While effective in practice, the use of added steel plates in retrofitting is prone to corrosion, resulting in higher future maintenance costs. Consequently, there is a growing focus on employing an alternative material as fiber-reinforced polymer (FRP) [28, 29]. Previous studies indicate that bonding FRP sheets to damaged members effectively enhances the load-carrying capacity, ductility, and stiffness of the structure. This technique effectively improves the flexural and shear performance of damaged RC structures [28, 30–34]. FRP materials composed of polymer fibers and an epoxy resin matrix are corrosion-resistant. Additionally, they exhibit exceptional strength and rigidity in the direction of the fibers.

In corrosive environments, stirrups typically corrode before longitudinal reinforcement due to the relatively small thickness of the cover to the concrete [35–37]. Engineers are increasingly adopting epoxy-bonded FRP products for strengthening applications due to their superior properties and non-corrosive nature [38]. Also, numerous methods such as the application of plates, steel sheets, and fiber-containing concrete have been established to repair and strengthen corroded RC elements [39]. Exposing epoxy-bonded metals to harsh environments like de-ionized water, urea solution, and saltwater affected their performance, and revealed alterations in interfacial capacity due to plasticization and substrate corrosion [40]. Dawood and Rizkalla conducted experiments to assess the capacity of the bond between CFRP and reinforcement under harsh environmental conditions [41]. Experiments were carried out by Hongming Li and Jin Wu to assess the shear performance of RC beams containing corroded stirrups, which were strengthened with CFRP [42]. The present study involved constructing specimens with embedded stirrups undergoing accelerated corrosion, leading to varying levels of corrosion damage. Also, the focus was on strengthening RC beams containing corroded stirrups, considering different corrosion cases and FA content. The strengthening included full wrapping of CFRP sheets externally bonded to simply supported square cross-section RC beams subjected to central point load. Finally, the performance of corroded and strengthened beams was compared based on shear capacity, crack width, and load–deflection response indicating that the strengthened specimens exhibited higher stiffness under service load conditions.

Significance of research

Prior studies have examined the flexural performance of RC beams with corrosion of main reinforcement, but the analysis of the performance for FA blended RC beams with corroded stirrups and the development of a comprehensive calculation model for shear capacity is still lacking. There is also a scarcity of literature on the strengthening of RC beams blended with FA and corroded stirrups by CFRP. This paper investigates the shear strength of RC beams made with FA and containing corroded stirrups. Also, evaluates the failure mode and efficiency of CFRP shear-strengthening methods to address existing gaps in the literature.

Experimental program

Figure 1 illustrates a clear understanding of the experimental methodology employed in this study.

Materials properties and specifications

Cement and FA

Ordinary Portland cement of 53 grade and F class FA sourced from the thermal power station at Nashik in Maharashtra, India, was chosen as the binding agent following Indian standards (IS): 12,269:2013 [43] for concrete matrix production.

The properties of both cement and FA by following the Indian standard code are indicated in Tables 1 and 2. The specific gravity value for cement was 3.15 and FA was 2.15.

Fine aggregate (crushed sand) and coarse aggregate (CA)

The properties of both crushed sand and CA by following the Indian standard code are indicated in Table 3.

Reinforcement

The tensile characteristics of eight randomly chosen corrosion-free reinforcement bars were assessed following both the Indian standard: 1608–2005 [48] and the American standard: ASTM A370 [49]. Table 4 presents the determined mechanical properties of reinforcements.

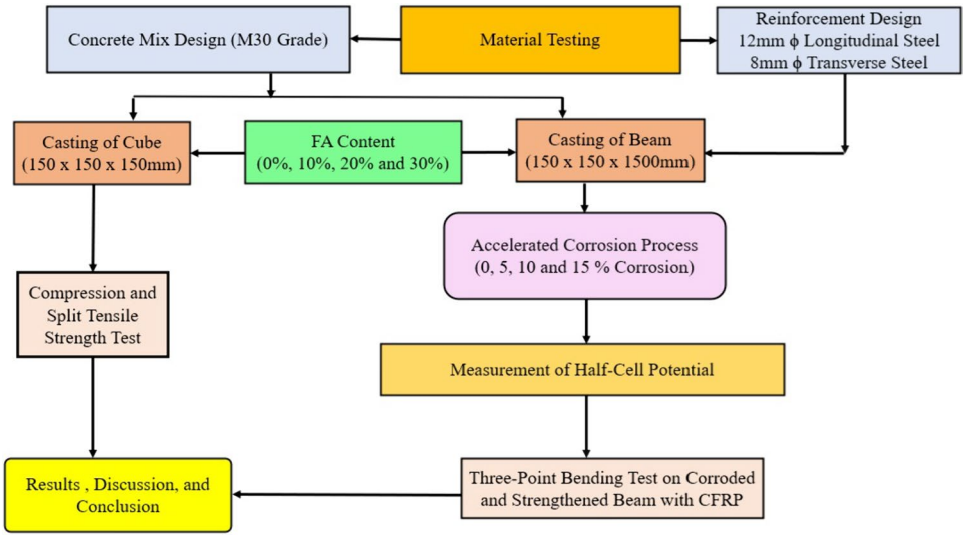

Fig. 1 Flow Chart for Experimental methodology

Table 1 Chemical Characteristics of *OPC* and *FA*

Material	Compound, % by weight									
	SiO_2	Al_2O_3	Fe_2O_3	CaO	SO_3	MgO	K_2O	Na_2O	TiO_2	LOI
Cement	21.0	05.0	3.6	63.0	2.5	0.88	0.45	0.15	0.16	–
FA	56.0	25.0	08.0	02.0	1.8	1.92	0.71	1.90	1.70	03.0

Table 2 Physical Properties of *OPC* and *FA*

Experimental Tests	Results	Standard specification	References
Cement			
Consistency	30%	25 to 35%	IS 5513 and IS 4031 [44, 45]
Specific surface area (m^2/kg)	230	Not > 225	IS:12,269 [43]
Setting time (Initial) in Minutes	35	Not > 30	IS:12,269 [43]
Setting time (Final) in Minutes	600	Not > 600	IS:12,269 [43]
FA			
Specific Surface Area (m^2/kg)	330	Minimum of 225 mm	IS:3812: (Part-I) 2013[46]
Particle Size > 45 µm	6.25%	Maximum of 34%	IS:3812: (Part-I) 2013[46]

Table 3 Properties of both crushed sand and CA

Material	Grading	Bulk density (kg/m^3)	Particle size	Specific gravity	Water absorption (%)
Crushed Sand	Zone II, as per IS 383 [47]	1750	Passing through a 4.75 mm sieve	2.65	0.8
CA	Angular-graded	1780	Maximum size of 20 mm	2.75	0.6

Strengthening materials

Various materials, including putties, primers, epoxy resins, and CFRP sheets, are utilized in FRP strengthening systems. Putty is applied to fill surface voids, like bug holes, ensuring a smooth bonding surface and preventing bubble formation during resin curing. Epoxy resins were used as binders for CFRP wrapping due to their excellent mechanical properties, good adhesion to concrete, and chemical resistance. The resin acts as an adhesive, filling and securing reinforcing fibers, providing an effective load transfer path. Epoxy resins are typically composed of a mixture of epoxy monomers and oligomers. These components provide the base material for the binder. Epoxy resins are characterized by their low

Table 4 Mechanical Properties of Reinforcement Bars

Sample bars	Φ (mm)	Area (mm^2)	f_y (MPa)	f_u (MPa)	Elastic tensile modulus (GPa)	ε_y	ε_u	Percentage elongation
1	12	113.09	509.91	610.29	200	0.0014	0.18	18
2	12	113.09	519.13	609.30	200	0.0013	0.17	17
3	12	113.09	515.20	611.00	200	0.0015	0.18	18
4	8	50.27	519.13	609.30	200	0.0013	0.19	19
5	8	50.27	512.37	614.20	200	0.0014	0.18	18
6	8	50.27	510.45	611.40	200	0.0015	0.18	18

Φ: diameter of reinforcement, f_y: average yield strength, f_u: ultimate strength, ε_y: yield strain, ε_u: ultimate strain

Fig. 2 Strengthening materials, (**a**) Resin and hardener, (**b**) *CFRP* Sheet

viscosity in liquid form, allowing them to impregnate the carbon fiber fabric effectively. The phase composition of the resin includes the various molecular structures of epoxy molecules, which determine properties such as viscosity, flexibility, and adhesion. An epoxy resin and a hardener mixed, undergo a chemical reaction that results in a strong and durable polymer matrix. A hardener initiates the cross-linking reaction that transforms the liquid resin into a solid polymer network. Common hardeners include polyamines and polyamides. The phase composition of the hardener involves the various functional groups and molecular structures that participate in the chemical reaction with the epoxy resin. This reaction forms covalent bonds, leading to the formation of a three-dimensional network structure, which provides the cured epoxy with its mechanical strength and durability. Adhesives bond the concrete surface and multiple layers of CFRP laminate, creating a path for the shear load. Protective coatings safeguard cured CFRP reinforcement from environmental damage. Figure 2 shows strengthening materials including resin, hardener, and *CFRP* Sheet.

The *CFRP* sheets typically exhibit high elastic modulus and tensile strength with a low weight-to-strength ratio. The mechanical properties of *CFRP* sheets are given in Table 5.

Table 5 Mechanical Properties of *CFRP*

Material	Fiber Weight /g /m^2	Tensile strength (MPa)	Tensile modulus of elasticity (MPa)	Ultimate elongation (%)
CFRP	200	3060	2.1×10^5	1.6

Table 6 Mechanical Properties of Epoxy resin

Material	Compressive strength (MPa)	Tensile strength (MPa)	Tensile modulus of elasticity (MPa)	Ultimate elongation (%)
Epoxy resin	75.4	35.5	2040.6	2.1

CFRP sheets, bonded with epoxy resin and hardeners, were used for strengthening applications on concrete specimens. The mechanical properties of epoxy resin (adhesive glue) are tabulated in Table 6.

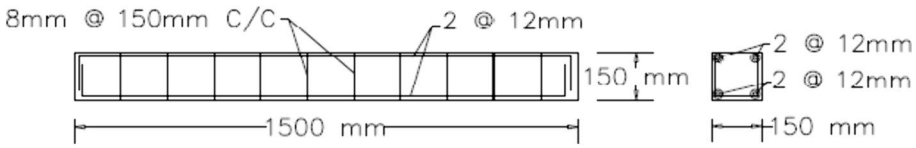

Fig. 3 Beam reinforcement details

Table 7 Concrete mix proportion

Materials in kg/m^3	Mix-I	Mix-II	Mix-III	Mix-IV
Cement	474	426.6	379.2	331.8
CA	1085	1085	1085	1085
Crushed sand	748	748	748	748
Water	186	186	186	186
FA	0.00	47.4	94.8	142.8

Water

Concrete ingredients were mixed, and cubes, cylinders, and beams were cured using locally available ordinary portable water.

Mix design and sample preparation

The study utilized eight RC beams, classified into strengthened and un-strengthened groups. The reference specimen (CB0) remained free from corrosion and strengthening. Subsequently, the corroded group consists of three beams (CB1, CB2, and CB3), and a CFRP-strengthened group consisting of four beams (SB0, SB1, SB2, and SB3). For the casting of beams, a custom mold with 150 mm × 150 mm × 1500 mm dimensions was fabricated and used. The specimen used 8 mm diameter thermo mechanically treated bars (TMT) as stirrups, spaced at 150 mm, with bottom and top reinforcement comprising two 12 mm diameter steel bars each. After completing the reinforcement cage, the 12 mm diameter steel bar (main bar) and the 8 mm bar stirrups were welded to expedite stirrup corrosion. Refer to Fig. 3 for reinforcement and geometric details of the specimens.

All RC beams were designed for M30 grade concrete following IS 456:2000 [50] and IS 10262:2019 [51]. The design of mix-I, mix-II, mix-III, and mix-IV refers to 0%, 10%, 20%, and 30% FA, and proportions for all the mixes are given in Table 7**.**

All the molds were cleaned and the surface was made smooth before use by applying grease or oil to facilitate easy de-molding. The cement and fine aggregate are blended in a laboratory pan-type mixer until a uniformly colored mixture is achieved, then introduced the coarse aggregates, are mixed thoroughly with all aggregates, and then water. The concrete was poured into the molds of cubes (150 mm cubes), cylinders (150 mm diameter, 300 mm depth), and beams (150 × 150 × 1500 mm) in three layers and compacted. These specimens have varied dosages of 0%, 10%, 20%, and 30% FA for CS, split tensile strength (STS), and flexural strength (FS) testing cast respectively. Figure 4 shows the sample preparation including mixing, casting, and curing of specimens.

A uniform water-to-cement content ratio of 0.39 was maintained for all mixes. Specimens were molded at temperatures varying from 21 to 45 °C, with humidity levels ranging approximately between 47 and 63%. The concrete-filled mold was kept in place for 24 h to allow the concrete to set. After 24 h, all the mold components were removed, leaving the beam specimen exposed. The curing of all test specimens was carried out by submerging the specimen in clean fresh water in a tank for 28 days.

Fig. 4 Sample preparation: **a** Mixing, **b** Casted sample **c** Curing

To mitigate the time-dependent CS effect, the transfer of all RC beams to the corrosion pool took place after a curing period of 28 days. Out of eight beams, six of them were intended for corrosion testing, and the remaining two were used as controlled beams. The average CS and STS of the specimen were determined using test results obtained from specimens evaluated on the same day as the commencement of beam specimen testing. Table 8 provides information on all the beams cast with different FA percentages (0%, 10%, 20%, 30%). The targeted corrosion levels for the reinforcement in each beam were set at 5%, 10%, and 15%.

Accelerated corrosion process (ACP) for stirrups

To expedite the corrosion process in the test specimens, an ACP was employed [21, 22, 52–60]. Figure 5 shows the schematics of the ACP. After curing, the test beams were immersed in a tank containing a 5% NaCl solution, by weight of the water. Throughout the testing, the depth of the water was kept constant at the beginning of each setup. In this setup, a stainless-steel plate served as the cathode (negative terminal) of the circuit, while a copper wire connected all the stirrups, acting as the anode (positive terminal). With a 26 V DC power flowed from the anode to the cathode and led to the oxidation of stirrups, involving loss of electrons and resulting in corrosion [61]. Maintaining a constant current density of 270 μA/m^2, specimens CB1-CB3 and SB1-SB3 underwent corrosion for durations of 4, 8, and 10 days, respectively to achieve 5, 10, and 15% of stirrup corrosion [61]. The main steel and stirrups were insulated by applying epoxy grout at the junction to prevent corrosion of the main steel and to control the corrosion rate of the stirrups. Faraday's law, given by Eq. 1, correlates mass loss with a magnitude of electrical current (DC), and exposure duration was used to calculate the theoretical mass loss of stirrups due to corrosion. [42].

$$M = \frac{ITA}{NF} \tag{1}$$

where I is the impressed DC in Ampere, T is the duration of exposure in seconds, $A = 55.847$ g is the atomic mass of iron, $N = 2$ is the number of electrons transferred during the

Table 8 Measured weight corrosion level of stirrups

Beam	FA (%)	Targeted corrosion level (%)	Measured corrosion level	Measured corrosion level/design corrosion level
CB0	0	0	0	0
CB1	10	5	5.20	1.04
CB2	20	10	10.50	1.05
CB3	30	15	16.10	1.07
SB0	0	0	0	0
SB1	10	5	5.30	1.06
SB2	20	10	10.60	1.06
SB3	30	15	16.10	1.07

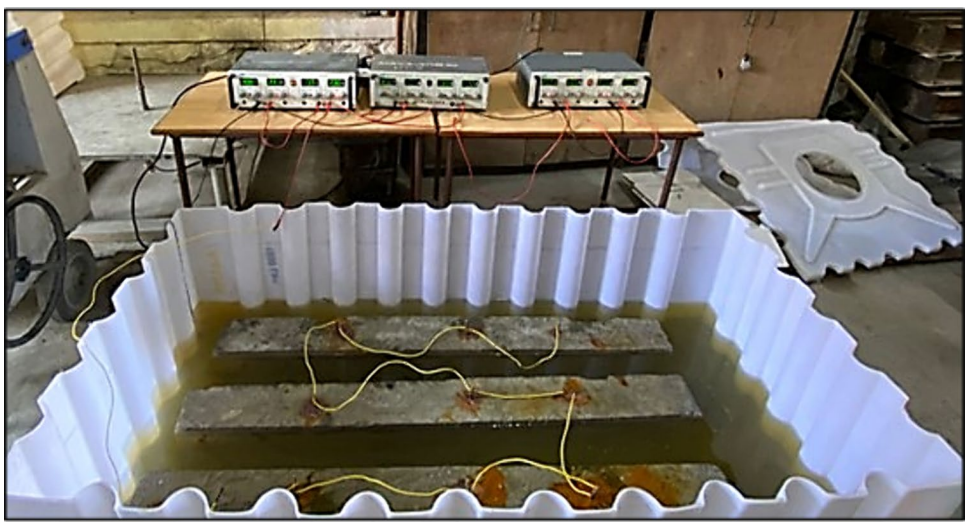

Fig. 5 ACP setup

Fig. 6 Corroded beam specimen

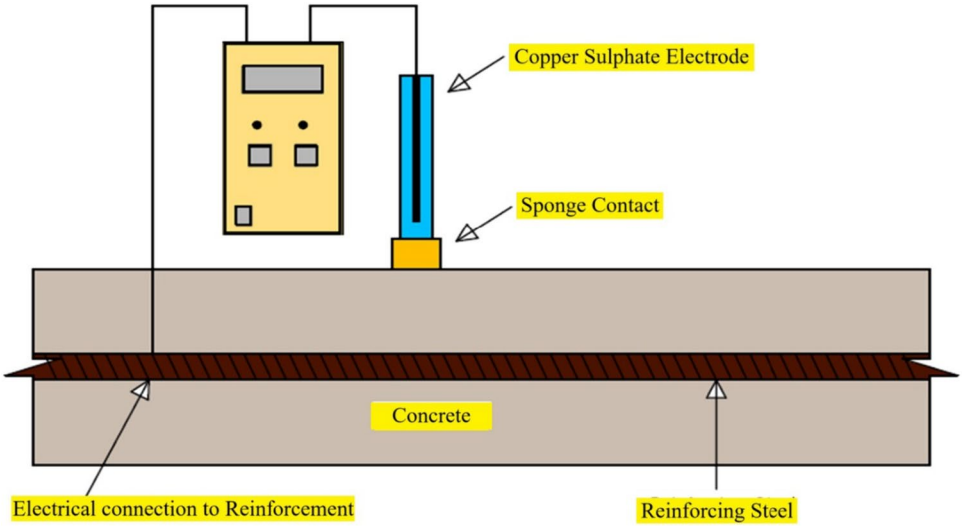

Fig. 7 Schematic illustration of the HCP test

corrosion reaction for iron, and $F = 96.500$ C/equivalent is Faraday's constant. This allows for accelerated completion of steel bar corrosion in a short duration of time. Figure 6 shows a typical corroded beam specimen after ACP.

Half-cell potential (HCP) test

The present study utilizes the HCP test to assess the probability of corrosion of reinforcement embedded within RC members was evaluated following ASTM C876:15 [62]. Figure 7 shows a schematic illustration of the HCP test.

The potential difference is influenced by the resistivity of the concrete and the thickness of the cover to the reinforcement, and it will rise concurrently with both factors [63]. The FA acts as a corrosion inhibitor and enhances the resistivity of concrete during extended curing periods [64–66]. With the escalation of the FA percentage, there is a corresponding shift toward higher positive values, indicating a nearly negligible corrosion potential. This was due to the pozzolanic reaction of FA, which refines the micro-pore structure, thereby impeding the infiltration of aggressive agents like oxygen and moisture and ultimately preventing the corrosion of the reinforcement. Table 9 displays the range of HCP values for the reinforcement and reveals that the beam with 20% FA exhibited a less negative value than the beam with 0%, 10%, and 30% FA, indicating more corrosion resistance.

Table 9 HCP values of reinforcement

Beam Group	Beam	FA Content in percentage	Range of Potential Values (mV, SCE)
Group-I	CB0	0	-170
	CB1	10	-190 to -260
	CB2	20	-200 to -290
	CB3	30	-215 to -370
Group-II	SB0	0	-172
	SB1	10	-190 to -260
	SB2	20	-200 to -290
	SB3	30	-215 to -370

The concrete mixture incorporating FA displays an HCP that is more negative (cathodic) than a concrete mixture without FA. A more negative potential signifies increased corrosion resistance, implying that the inclusion of FA in the concrete has enhanced the durability and safeguarded the reinforcing steel. Interestingly, the FA systems, particularly those with 10% and 20%, demonstrated noteworthy voltage data values compared to OPC, indicating their superior corrosion resistance properties. Ha et al. reported a similar

observation [54]. On the contrary, surpassing a 20% FA content resulted in premature cracking in the concrete, signifying the unfavorable properties associated with this level of FA content. In the presence of water, FA reacts with calcium hydroxide ($Ca(OH)_2$), resulting in the formation of an additional calcium silicate hydrate (C–S–H) gel, as indicated by these observations. The C–S–H gel formed can compact the microstructure of concrete, offering potential mitigation against corrosion. Additionally, the calcium oxide (CaO) present in FA serves as an alkaline buffer, aiding in sustaining higher pH levels in the concrete. This promotes the passivation of the steel reinforcement and reduces the corrosion rate. The presence of FA in the system can be attributed to the primary hydration reaction, represented as follows:

$$2\left(3CaO.SiO_2\right) + 6H_2O \rightarrow 3CaO.2SiO_2.3H_2O + 3Ca(OH)_2 \quad (2)$$

In the presence of water, FA within the concrete has the potential to react with $Ca(OH)_2$, leading to the formation of C-S–H. Moreover, there exists an additional secondary hydration reaction, which can be formulated as follows:

$$3Ca(OH)_2 + 2SiO_2 + H_2O \rightarrow 3CaO.\,2SiO_2.\,3H_2O \quad (3)$$

The existence of this secondary C-S–H fills the substantial capillary voids, thereby improving the corrosion resistance properties.

Strengthening methodology

Surface preparation was conducted before the bonding of CFRP sheets to the concrete surface as per the guidelines given in ACI 546R [67] and ICRI 03730 [68]. The concrete surface was cleaned with the help of sandpaper to remove existing unsound material that may interfere with the bond between the FRP system and the concrete. Before applying the CFRP system, the corners of the beams were rounded and smoothed following ACI 440.2R 08 [69] to approximately 13 mm radius to avoid stress concentrations. After cleaning the surface, putty was used to make the surface smooth and fill all voids from the beam surface. The Putty took 24 h to dry. After drying the putty, primer was applied on the beam surface on which CFRP will be applied. The primer was made by mixing resin and hardener in a plastic container. The resin and hardener proportion were 1:2. It took 24 h for drying. The primer was applied axially, followed by impregnating with saturating resin and bonding CFRP sheets. The saturating resin was layered onto the primer. CFRP was cut to 300 mm width before resin curing, placed on the epoxy-coated surface spaced at 300 mm intervals, and resin was pressed through the fabric roving. Air bubbles trapped at the epoxy and concrete or epoxy and fabric interface were removed. Full wrapping of CFRP was applied over the saturated resin area at room temperature, and a protective coating was added to the CFRP sheet to shield the bonded FRP reinforcement from environmental damage. The beams reinforced with CFRP sheets were cured for 5 days at room temperature before testing. Figure 8 shows a retrofitting procedure which was used for this research. In this research, all four sides of the beams are wrapped and this scheme is more efficient than two-side and three-side wrapped schemes.

Findings and discussion

CS and STS

The compression testing machine (CTM) is employed to assess the CS of concrete using standard cube-size molds following a 28-day curing period. Testing was conducted on three cubes following the IS: 516:1959 guidelines [70], and the individual strength of each cube as well as the average CS were recorded. Additionally, cylinders were tested using a 2,000 kN capacity CTM. Three cylinders were subjected to testing following IS: 5816–1959 guidelines [71], and the individual and average split tensile strength (STS) were noted. Figures 9 and 10 show the experimental setup for CS and STS of concrete.

It was noted that the CS increased by 3.59% and 5.57% when incorporating 10% and 20% FA, respectively. However, CS decreased by 2.17% when 30% FA was used, compared to 0% FA, after a 28-day curing period. The CS exhibited marginal improvement up to a 20% cement replacement with FA, and further replacement beyond 20% resulted in a slight decrease in strength at 28 days. However, up to 30% FA demonstrated the desired strength for M30-grade concrete. This trend was also observed in STS. Figures 11 and 12 present the CS and STS of concrete with varying FA percentages after a 28-day curing period.

The enhancement in both CS and STS results from the pozzolanic characteristics of FA. Because of pozzolanic properties and the tiny particle size of FA, voids between the cement particles are filled by the FA, enhancing overall density and interlocking particles, and resulting in reduced porosity [21, 72]. However, excessive utilization of FA (beyond 30%) reduced the CS and STS of concrete. Also, excessive utilization of FA leads to a reduction in the reactivity and overall performance of concrete [22]. Hence, the present study was restricted to utilizing the FA beyond 30%.

Three-point bending test

The experimental setup and the schematic diagram of the three-point flexural test setup are presented in Fig. 13a and b. A load was applied at the rate of 0.05 kN/s to the specimens

Fig. 8 **a** Putty Filling, **b** Prime coating, **c** Saturated coating **d** Fiber laminate

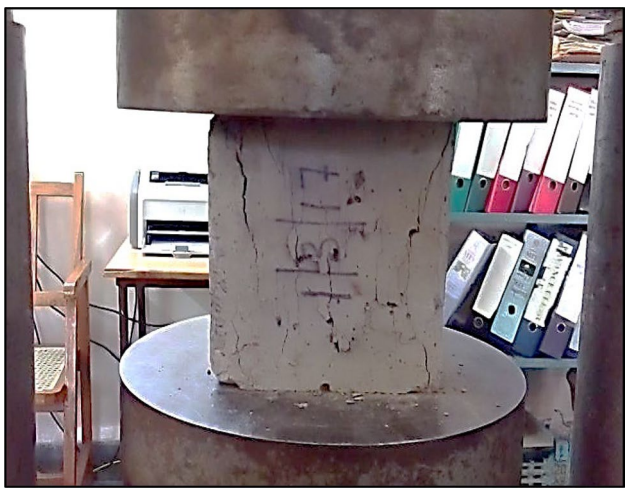

Fig. 9 CS test

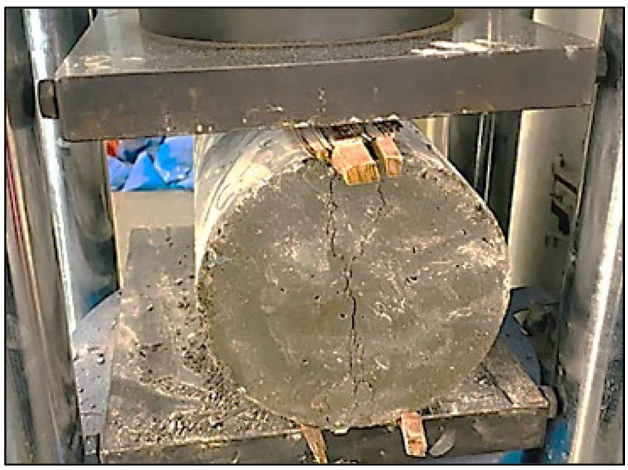

Fig. 10 STS test

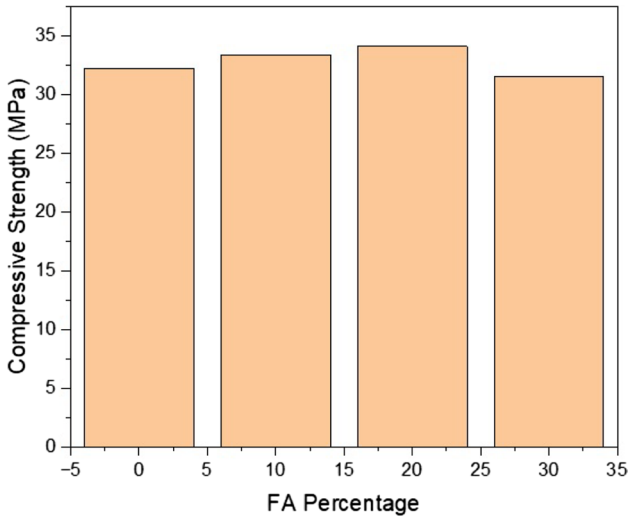

Fig. 11 Effect of FA percentage on CS

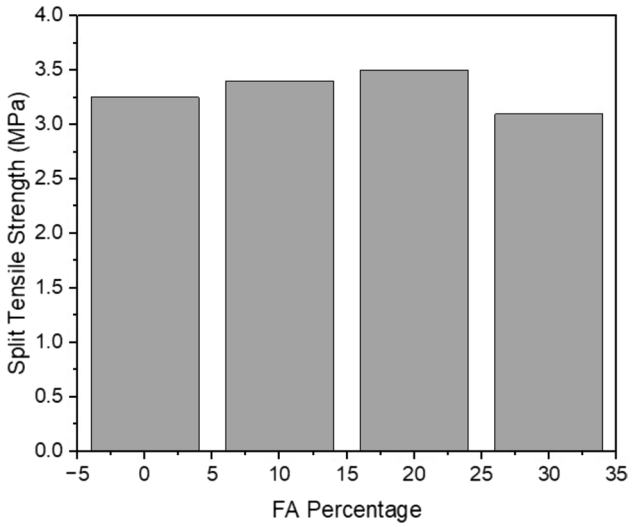

Fig. 12 Effect of FA percentage on STS

and a dial gauge was fitted during testing to measure deflections below the load at the mid-span of the beams.

Mid-span deflection

The load at first crack, load at failure, and cracking pattern of the beams were recorded. Before reaching the cracking load, the specimen exhibited minimal deflection, and the load–deflection relationship followed a linear pattern. Upon reaching the ultimate load, the specimen experienced a sudden loss of bearing capacity, indicating a brittle failure. The corrosion of the reinforcement leads to a reduction in the stiffness of the strengthened beam as compared to CB0. An increase in the corrosion level of stirrups, led to a reduction in the effective area of the stirrups, causing a decrease in the stiffness of the corroded, unstrengthened beam. This reduced stiffness of the corroded RC beam was improved by CFRP wrapping. The ultimate deflection at the mid-span of CB0 was 6.5 mm, while the ultimate deflection of SB3 was 4.3 mm, indicating a 33.84% decrease compared to CB0. The ultimate deflection of SB3 reached 4.3 mm, which was 17.30% higher than the ultimate deflection of SB0. The load–deflection plot at mid-span is depicted in Figs. 14 and 15.

Table 10 presents the experimental results for load–deflection and crack width of the specimens. In the present study, it was observed that the stiffness of the corroded RC beam is not affected significantly due to CFRP strengthening with an increase in the corrosion level of stirrups which is in contrast to Hongming Li's study [42]. However, the stiffness and ultimate strength of the strengthened corroded RC beam decreased with an increase in the stirrup corrosion level. Furthermore, it has been noted that the stiffness of the RC beam decreases with an increase in corrosion level. This is because of the decrease in yield strength and corresponding displacements of the corroded RC beam. Also, reinforcement bar corrosion induces early yielding and concrete deterioration, amplifying crack opening under load, ultimately reducing displacement at yield strength [5, 73, 74]

Loss of stirrups owing to corrosion

After the completion of the loading test, the stirrups were extracted from the RC beams and cleaned, ensuring the removal of concrete and corrosion products from their surface. After cleaning with a 12% HCl solution, the corroded stirrups were rinsed with water, neutralized with lime water, and rinsed again. Dried for at least 4 h, their weight was then measured on an electronic balance. The measurement of all corroded steel bars followed the procedure outlined in ASTM G1-03 [75], from which the steel corrosion, denoted as P_{cor}, i.e., the average weight-loss level, was subsequently calculated [76] by Eq. 4.

$$p_{cor} = \frac{M_0/L_0 - M_1/L_1}{M_0/L_0} \tag{4}$$

where P_{cor} represents the percentage of steel corrosion in the bars; M_0 and L_0 denote the mass and length of the uncorroded steel bars, respectively. The uncorroded steel bars from the control beam B0 were selected as the reference for M_0 and L_0. Similarly, M_1 and L_1 denote the mass and length of the corroded steel bars in the tested beams. Measurements of L_0 and L_1 were conducted using a Vernier caliper. The corrosion levels of the steel bars as measured are presented in Table 7.

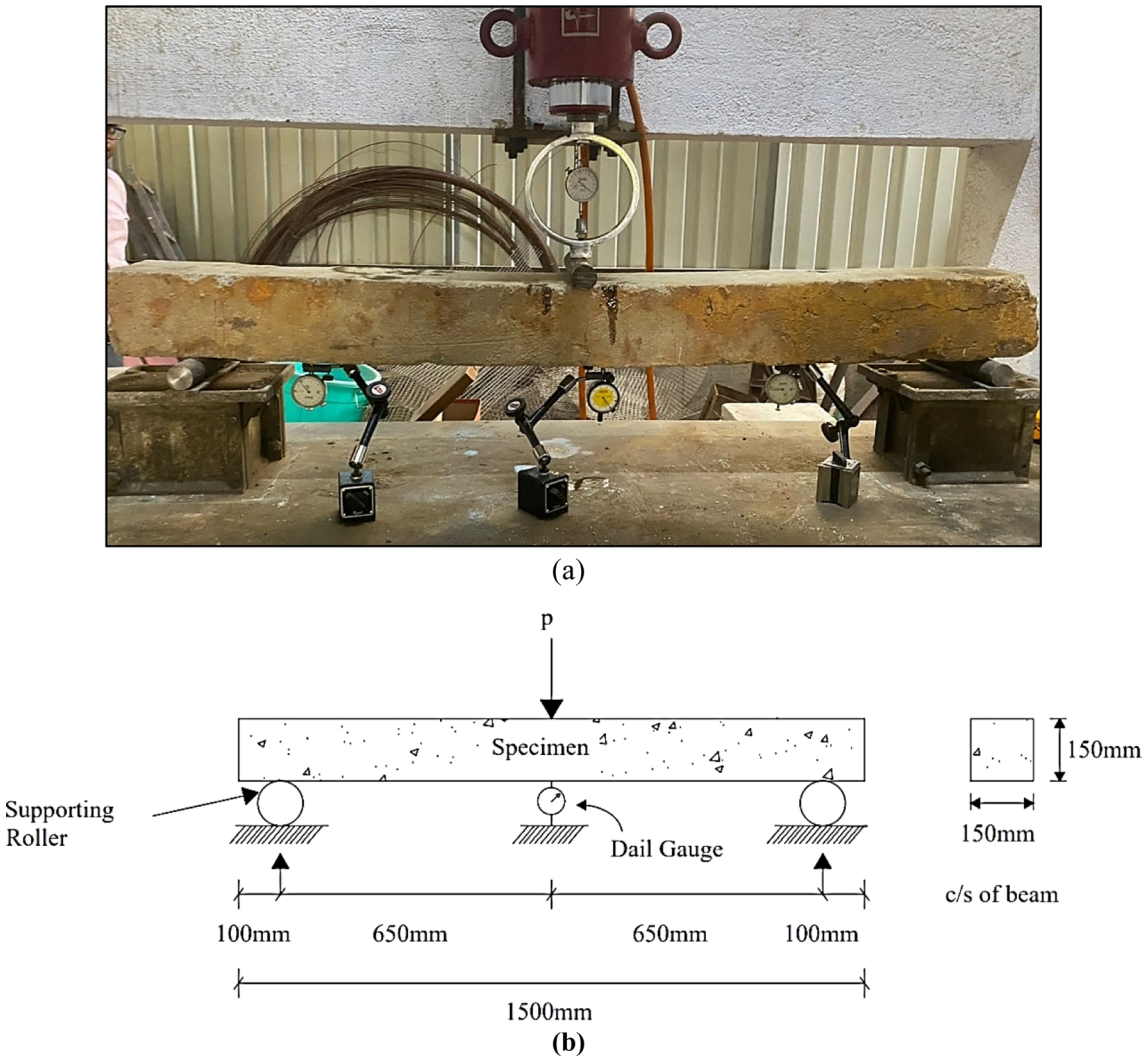

Fig. 13 Three-Point Bending Test: **a** Experimental setup, **b** Schematic diagram of a three-point flexural test setup

Surface-cracking

Diagonal cracks confirm shear pressure failure and there was sudden widening of cracks during damage. Corroded beams experienced shear compression failure, and most of the cracks intersected with diagonal cracks perpendicular to the length of the beam. The development of these diagonal cracks in the shear bending zone depends on the tensile strength of concrete under multiaxial stress. The development of load cracks remained consistent and which is unaffected by variations in corrosion expansion cracks under different stirrup corrosion conditions. Under a small load, vertical cracks emerged directly beneath the applied load in the bending tension zone. As the load increased, additional vertical cracks appeared in the shear flexural zone. All test beams exhibited shear compression failure. As diagonal cracks formed, deformation and stirrup strain in each beam quickly increased. This likely occurred due to damaged concrete sections because of stirrup corrosion and weakening their ability to resist the crack development. While pre-crack stirrup strain was similar across beams, its location varied significantly afterward, aligning with the experiment's observations. Notably, high strain values were found where stirrups intersected the diagonal cracks. Due to the crack location appearing between the support and load point, the strain value at both ends exceeded the strain value mid-span of the beam. Importantly, despite reaching the ultimate load in the corroded beam, none of the stirrups in any test beam yielded. The same observations were noticed by Hongming Li's [42]. The maximum width of diagonal cracks was measured at 1.4 mm and 1.6 mm for SB2 and SB3 respectively as well as the maximum crack width for the strengthened beam ranged from 1.2 to 1.60 mm. As the RC beam reached its cracking point, CFRP strain suddenly increased, demonstrating its immediate contribution in halting further crack

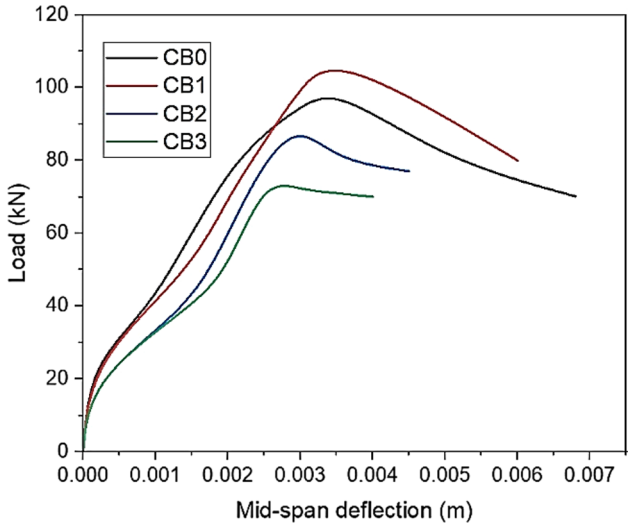

Fig. 14 Load deflection curve for corroded non-strengthened beams (CB0-CB3)

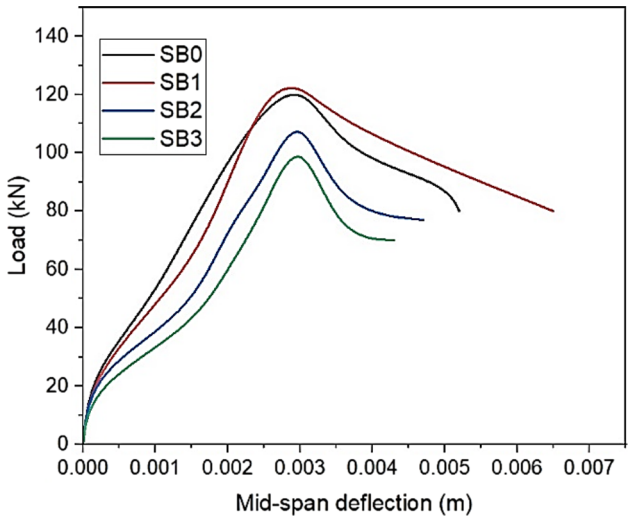

Fig.15 Load deflection curve for corroded strengthened beams (SB0-SB3)

propagation. The specimens failed due to CFRP debonding before achieving its ultimate strength and the concrete was crushed. Figure 16 illustrates the failure mode for both corroded and strengthened beams.

Experimental shear capacity of strengthened corroded RC beams

It was observed that the shear capacity determined by experimental tests on the strengthened beams exceeds the analytical value. The critical diagonal crack in beam SB3 occurred at its ultimate load of 110 kN, marking a 15.38%, 12%, and 6.78% reduction compared to the ultimate loads in beams SB0, SB1, and SB2, respectively. However, the shear capacity of the RC beams displayed an increasing trend up to a 5% corrosion level, attributed to the pressure developed by corrosion products. Beyond the 5% corrosion level, the shear capacity of the RC beams did not show a further increase with the increase in the stirrup corrosion levels. The addition of CFRP sheets substantially enhanced the shear capacity of corroded beams. The increase in shear strength for the RC beam reinforced with CFRP sheets was greater than 27.27% for SB3 in comparison to CB3, and 23.72% for SB2 compared to CB2. The same growth trend in shear strength of the RC beam strengthened with CFRP sheets was observed by Hongming Li [42].

Analytical shear capacity of strengthened corroded RC beams

For the strengthened beam, the recommended shear capacity was calculated as the combined contributions of concrete, stirrups, and CFRP. The theoretical value of V_{Cal} was determined using established methods outlined in ACI318-14 [77] and ACI 549.4R-13 [78] by Eq. 5

$$V_{\mathrm{Cal}} = V_c + V_s + V_f \tag{5}$$

where, V_{Cal} represents the shear bearing capacity of the strengthened beams, while V_c, V_s, and V_f denote the

Table 10 Experimental results of the specimens

Beam	Corrosion level of stirrups (%)	Ultimate Load (kN)	Mid-span deflection (mm)	Maximum width of bending cracks (mm)	Maximum width of oblique cracks (mm)
CB0	0	100	6.8	0.20	1.0
CB1	5.20	110	5.0	0.24	1.2
CB2	10.50	90	4.5	0.26	1.4
CB3	16.10	75	4.0	0.28	1.6
SB0	0	130	5.2	0.30	1.4
SB1	5.30	125	6.5	0.27	1.2
SB2	10.60	118	4.7	0.28	1.4
SB3	16.10	110	4.3	0.31	1.6

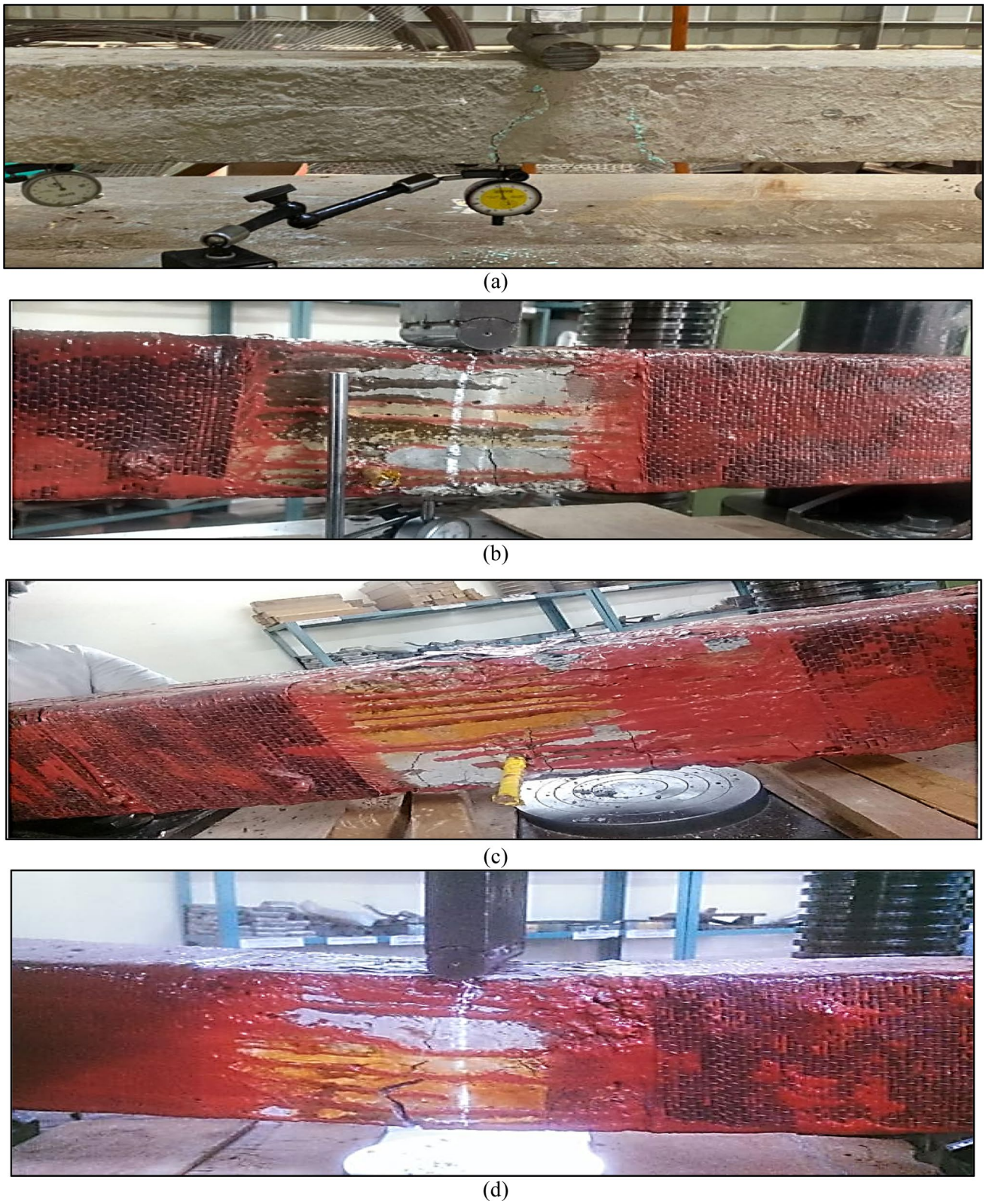

Fig. 16 Beam failure mode-**a** Beam-SB0, **b** Beam-SB1, **c** Beam-SB2, **d** Beam-SB3

shear bearing capacities of the concrete, steel, and CFRP, respectively.

The expression for the calculation of V_f is given by Eq. 6 as follows [69]:

$$V_f = \phi_f A_f f_{\mathrm{Fe}} (\sin\beta + coc\beta) d_f / s_f \quad (6)$$

The relative reduction coefficient, denoted as ϕ_f, is a key parameter in the context of this study. The total cross-section area of the double-limb CFRP band, represented by A_f, is determined as $A_f = 2nt_f\omega_f$, where n stands for the number of CFRP layers, t_f is the layer thickness of the CFRP, and ω_f is the width of the CFRP strip. The CFRP angle is denoted by β, and d_f represents the effective height, while s_f corresponds to the spacing for the CFRP band. The effective strain in the CFRP, denoted as ε_{fe}, is calculated using the expression $f_{Fe} = E_f\,\varepsilon_{fe}$; E_f, where E_f is the elastic modulus of the CFRP. The calculation of ε_{fe} is based on ACI440.2R-08 [69]. Utilizing this formula, the shear-bearing capacities of seven specimens were computed. The tabulated results in Table 11 demonstrate a favorable concordance with the experimental findings.

The calculated value exhibited a mean deviation of 1.095 from the test value, with a standard deviation of 0.095 and a coefficient of variation of 0.085. Figure 17 shows experimental results (shear force) of strengthened beam with error bars.

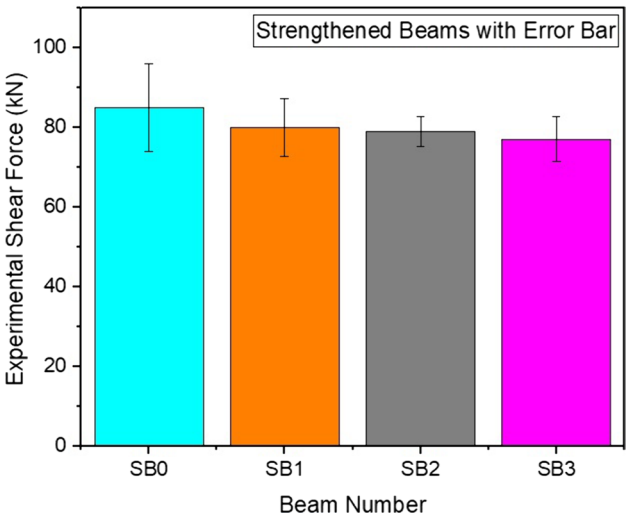

Fig. 17 Experimental shear force with error bars

Conclusion

The presentation focused on the shear behavior of *RC* beams following stirrup corrosion. The subsequent observations and findings drawn from the test results are as follows:

(1) The corrosion resistance of reinforcing bars within concrete is enhanced through the partial replacement of cement with FA. This improvement is attributed to a reduction in the corrosion current generated under a constant DC voltage. The research findings indicate that an elevated proportion of FA in concrete enhances its capability to withstand accelerated corrosion induced by the application of DC voltage and half-cell potential values.

(2) The study has identified that the optimal replacement proportion of cement with *FA* is 20%, resulting in improved CS and STS of the concrete. Nevertheless, beyond a 20% *FA* content results in a reduction in strength. It was observed that the inclusion and variation of FA did not exert a notable impact on the flexural and shear capacity of the RC beam. The shear capacity of corroded beams showed a marginal improvement when the stirrup corrosion level was below 5%. However, it diminished thereafter as the stirrup corrosion level surpassed 5%.

(3) The beams reinforced with CFRP sheets demonstrated a 23.07% increase in ultimate load capacity compared to the control beam CB0. Test outcomes indicated that complete CFRP wrapping on the deteriorated RC beams elevated load capacities by 9.1% to 23.1% in comparison to the control RC beam without corrosion.

Table 11 Analytical and Experimental results of the specimens

Beam	*CS*	*STS*	*fy*	Corrosion level of stirrups	Analytical shear force (V_{Cal})	Experimental shear Force (V_{Exp})	$\frac{V_{Exp}}{V_{Cal}}$
CB0	33.10	2.85	500	0	*NA*	72.00	*NA*
CB1	35.30	2.95	500	5.20	*NA*	77.20	*NA*
CB2	34.50	2.90	500	10.50	*NA*	70.10	*NA*
CB3	33.50	2.75	500	16.10	*NA*	63.00	*NA*
SB0	35.70	3.10	500	0	73.91	85.00	1.15
SB1	34.90	2.80	500	5.30	72.72	80.00	1.10
SB2	35.00	2.90	500	10.60	75.23	79.00	1.05
SB3	33.90	2.75	500	16.10	71.38	77.10	1.08

The enhancement in shear-bearing capacity was more pronounced through CFRP strengthening. The beams wrapped with CFRP exhibited increased stiffness, demonstrating that CFRP laminates contribute to additional load-carrying capacity.

(4) The failure modes of corroded beams revealed concrete crushing in the shear compression zone. The application of CFRP sheets to corroded RC beams proved effective in restraining the development and propagation of diagonal cracks, thereby delaying the onset of critical cracks. The failure of the specimen occurred due to the debonding of CFRP, followed by concrete crushing. It was noted that the CFRP did not reach its ultimate strength during the process. From the initiation of loading until the emergence of diagonal cracks, the shear deformation in each test beam remained minimal, and the stirrups experienced a limited range of strain increase. After the appearance of diagonal cracks, there was a notable increase in the deformation of each test beam, accompanied by a rapid rise in stirrup strain.

(5) The mean ratio of the test value to the calculated value was 1.095, with a standard deviation of 0.095 and a coefficient of variation of 0.085. The calculated results exhibited a favorable concordance with the experimental findings.

Limitations and future scope

While solely exploring the use of CFRP as external reinforcement, this study has made significant strides in clarifying critical questions and issues related to the shear behavior of corroded RC beams. Predicting the combined flexural and torsional behavior of corroded RC beams under shear and moment demands further experimental investigation. Future studies should focus on the influence of longitudinal reinforcement ratio, beam geometry, and the complex interaction of forces. Also, an experimental study on stress–strain distribution in the strengthened beams with different orientations of CFRP sheets needs to be addressed in the future. A finite element modeling needs to be used to predict and verify the experimental results.

Funding The authors declare there is no funding information available that could influence the work reported in this paper.

Data availability Data will be made available on request.

Declarations

Conflict of interest On behalf of all authors, the corresponding author states that there is no conflict of interest.

Ethical approval This article does not contain any studies with human participants or animals performed by any of the authors.

References

1. Azad AK, Shamsad A, Syed AA (2007) Residual strength of corrosion-damaged reinforced concrete beams. ACI Mater J 104:1. https://doi.org/10.14359/18493
2. Lin H, Zhao Y (2016) Effects of confinements on the bond strength between concrete and corroded steel bars. Constr Build Mater 118:127–138. https://doi.org/10.1016/j.conbuildmat.2016.05.040
3. Lachemi M, Al-Bayati N, Sahmaran M, Anil O (2014) The effect of corrosion on shear behavior of reinforced self-consolidating concrete beams. Eng Struct 79:1–12. https://doi.org/10.1016/j.engstruct.2014.07.044
4. Sathe S, Patil S, Bhosale A (2023) Effectiveness of fly ash as corrosion inhibitor for reinforced concrete beam under torsion. Innovat Infrastr Solut 8:275. https://doi.org/10.1007/s41062-023-01246-y
5. Sathe S, Patil S (2023) Experimental analysis and behavior of corrosion-damaged fly ash blended reinforced concrete beam under flexural loading. J Build Pathol Rehabilitat 8:97. https://doi.org/10.1007/s41024-023-00344-9
6. Sathe S, Patil S, Shete V (2023) An experimental study on flexural strength of corroded-reinforced concrete beam with fly ash. In: Sil A, Kontoni D-PN, Pancharathi RK (eds) Recent trends in civil engineering: select proceedings of ICRACE 2021. Springer Nature Singapore, Singapore, pp 87–96. https://doi.org/10.1007/978-981-19-4055-2_8
7. Campione G, Cannella F, Cavaleri L (2017) Shear and flexural strength prediction of corroded RC beams. Constr Build Mater 149:395–405. https://doi.org/10.1016/j.conbuildmat.2017.05.125
8. Gaikwad P, Sathe S (2023) Effect of fly ash on compressive strength, carbonation and corrosion resistance of reinforced concrete: a systematic review. World J Eng. https://doi.org/10.1108/WJE-07-2023-0240
9. Vishnudevan M, Thangavel K (2006) Evaluation of organic based corrosion inhibiting admixtures for reinforced concrete. Anti-Corros Methods Mater 53:271–276. https://doi.org/10.1108/00035590610692545
10. Fazayel AS, Khorasani M, Sarabi AA (2018) The effect of functionalized polycarboxylate structures as corrosion inhibitors in a simulated concrete pore solution. Appl Surf Sci 441:895–913. https://doi.org/10.1016/j.apsusc.2018.02.012
11. Ormellese M, Bolzoni F, Goidanich S, Pedeferri M, Brenna A (2011) Corrosion inhibitors in reinforced concrete structures part 3 – migration of inhibitors into concrete. Corros Eng, Sci Technol 46:334–339. https://doi.org/10.1179/174327809X419230
12. Kubo J, Tanaka Y, Page CL, Page MM (2013) Application of electrochemical organic corrosion inhibitor injection to a carbonated reinforced concrete railway viaduct. Constr Build Mater 39:2–8. https://doi.org/10.1016/j.conbuildmat.2012.05.010
13. Blankson MA, Erdem S (2015) Comparison of the effect of organic and inorganic corrosion inhibitors on the rheology of self-compacting concrete. Constr Build Mater 77:59–65. https://doi.org/10.1016/j.conbuildmat.2014.12.032
14. Söylev TA, Richardson MG (2008) Corrosion inhibitors for steel in concrete: state-of-the-art report. Constr Build Mater 22:609–622. https://doi.org/10.1016/j.conbuildmat.2006.10.013
15. Tahwia AM, Elgendy GM, Amin M (2022) Effect of environmentally friendly materials on steel corrosion resistance of sustainable UHPC in marine environment. Struct Eng Mechan 82:609–622. https://doi.org/10.12989/sem.2022.82.2.000
16. Nochaiya T, Suriwong T, Julphunthong P (2022) Acidic corrosion-abrasion resistance of concrete containing fly ash and silica fume for use as concrete floors in pig farm. Case Stud Constr Mater 16:e01010. https://doi.org/10.1016/j.cscm.2022.e01010

17. Tahwia AM, Elgendy GM, Amin M (2021) Durability and microstructure of eco-efficient ultra-high-performance concrete. Constr Build Mater 303:124491. https://doi.org/10.1016/j.conbuildmat.2021.124491
18. Wagale M, Dandin S, Bokil S, Sathe S (2023) Potential use of fly ash in structural fill application: a review. Environ Sci Pollut Res. https://doi.org/10.1007/s11356-023-30968-w
19. Sathe S, Zain Kangda M, Amaranatha GA (2022) Resistance against sulphate attack in concrete by addition of nano alumina. Mater Today Proc 60:294–298. https://doi.org/10.1016/j.matpr.2022.01.124
20. Banu ST, Chitra G, Awoyera PO, Gobinath R (2019) Structural retrofitting of corroded fly ash based concrete beams with fibres to improve bending characteristics. Aust J Struct Eng 20:198–203. https://doi.org/10.1080/13287982.2019.1622490
21. Van Nguyen C, Lambert P, Bui VN (2020) Effect of locally sourced pozzolan on corrosion resistance of steel in reinforced concrete beams. I J Civ Eng 18:619–630. https://doi.org/10.1007/s40999-019-00492-5
22. Revathi P, Nikesh P (2018) Effect of fly-ash on corrosion resistance characteristics of rebar embedded in recycled aggregate concrete. J Inst Eng Ser A. 99:473–483. https://doi.org/10.1007/s40030-018-0295-6
23. Harilal M, Rathish VR, Anandkumar B, George RP, Mohammed MSHS, Philip J, Amarendra G (2019) High performance green concrete (HPGC) with improved strength and chloride ion penetration resistance by synergistic action of fly ash, nanoparticles and corrosion inhibitor. Constr Build Mater 198:299–312. https://doi.org/10.1016/j.conbuildmat.2018.11.266
24. Kaplan G, Bayraktar OY, Memis S (2021) Effect of high volume fly ash and micro-steel fiber on flexural toughness and durability properties in self-compacting lightweight mortar (SCLM). Constr Build Mater 307:124877. https://doi.org/10.1016/j.conbuildmat.2021.124877
25. Qeshta IMI, Shafigh P, Jumaat MZ (2016) Research progress on the flexural behaviour of externally bonded RC beams, archives of Civil and mechanical. Engineering 16:982–1003. https://doi.org/10.1016/j.acme.2016.07.002
26. De Domenico D (2015) RC members strengthened with externally bonded FRP plates: a FE-based limit analysis approach. Compos B Eng 71:159–174. https://doi.org/10.1016/j.compositesb.2014.11.013
27. P. Sarker, M. Begum, S. Nasrin, Fiber reinforced polymers for structural retrofitting: A review, 2011.
28. Ramachandra Murthy A, Karihaloo BL, Priya DS (2018) Flexural behavior of RC beams retrofitted with ultra-high strength concrete. Constr Build Mater 175:815–824. https://doi.org/10.1016/j.conbuildmat.2018.04.174
29. Medeiros L, da Costa T, de Carvalho A, Pires JJ, Silva R (2023) Shear strengthening of fire-damaged reinforced concrete beams using NSM CFRP laminates. Eng Struct 287:116175. https://doi.org/10.1016/j.engstruct.2023.116175
30. Hasan MA, Akiyama M, Kojima K, Izumi N (2023) Shear behavior of reinforced concrete beams repaired using a hybrid scheme with stainless steel rebars and CFRP sheets. Constr Build Mater 363:129817. https://doi.org/10.1016/j.conbuildmat.2022.129817
31. Huang Z, Miao X, Shen J, Li H, Zhang J (2021) Experimental investigation on shear behavior of concrete beams with CFRP grid shear reinforcements. Structures 33:3081–3093. https://doi.org/10.1016/j.istruc.2021.06.023
32. R. Al-Hammoud, ; Khaled Soudki, T.H. Topper, Fatigue flexural behavior of corroded reinforced concrete beams repaired with CFRP sheets, (n.d.). https://doi.org/10.1061/ASCECC.1943-5614.0000144
33. Suffern C, El-Sayed A, Soudki K (2010) Shear strength of disturbed regions with corroded stirrups in reinforced concrete beams. Can J Civ Eng 37:1045–1056. https://doi.org/10.1139/L10-031
34. Ye Z, Zhang W, Gu X (2018) Deterioration of shear behavior of corroded reinforced concrete beams. Eng Struct 168:708–720. https://doi.org/10.1016/j.engstruct.2018.05.023
35. Zhang W, Ye Z, Gu X (2017) Effects of stirrup corrosion on shear behaviour of reinforced concrete beams. Struct Infrastruct Eng 13:1081–1092. https://doi.org/10.1080/15732479.2016.1243563
36. Li W, Huang Z, Huang Z, Yang X, Shi T, Xing F (2020) Shear behavior of rc beams with corroded stirrups strengthened using FRP laminates: effect of the shear span-to-depth ratio. J Compos Constr 24:4. https://doi.org/10.1061/(asce)cc.1943-5614.0001042
37. Ji Y, Hu Y, Zhang L, Bao Z (2016) Laboratory studies on influence of transverse cracking on chloride-induced corrosion rate in concrete. Cem Concr Compos 69:28–37. https://doi.org/10.1016/j.cemconcomp.2015.12.006
38. Xie JH, Hu RL (2013) Experimental study on rehabilitation of corrosion-damaged reinforced concrete beams with carbon fiber reinforced polymer. Constr Build Mater 38:708–716. https://doi.org/10.1016/j.conbuildmat.2012.09.023
39. Martí-Vargas JR, Serna P, Hale WM (2013) Strand bond performance in prestressed concrete accounting for bond slip. Eng Struct 51:236–244. https://doi.org/10.1016/j.engstruct.2013.01.023
40. Doyle G, Pethrick RA (2009) Environmental effects on the ageing of epoxy adhesive joints. Int J Adhes Adhes 29:77–90. https://doi.org/10.1016/j.ijadhadh.2008.02.001
41. Dawood M, Rizkalla S (2010) Environmental durability of a CFRP system for strengthening steel structures. Constr Build Mater 24:1682–1689. https://doi.org/10.1016/j.conbuildmat.2010.02.023
42. Li H, Jin W, Wang Z (2016) Shear performance of reinforced concrete beams with corroded stirrups strengthened with carbon fiber- reinforced polymer. ACI Struct J 113:51–61. https://doi.org/10.14359/51687913
43. Indian Standards, IS 12269 (2013) 53 grade ordinary Portland cement, bureau of Indian standard, BIS, New Delhi India 110002
44. Indian Standards, IS 5513 (1996) Specification for vicat apparatus, bureau of Indian standard, BIS, New Delhi India 110002
45. Indian Standards, IS 4031-4 (1988) Methods of physical tests for hydraulic cement, Part 4: determination of consistency of standard cement paste, Bureau of Indian Standard, BIS, New Delhi India 110002
46. Indian Standards, IS 3812-1 (2013) Specification for pulverized fuel ash, part 1: for use as pozzolana in cement, cement mortar and concrete, bureau of Indian standards, BIS, New Delhi India 110002
47. Indian Standards, IS 383 (2016) Coarse and fine aggregate for concrete- specification, bureau of Indian standard, BIS, New Delhi India 110002 (2016).
48. Indian Standards, IS 1608 (2005) Mechanical testing of metals - tensile testing, bureau of Indian standard, BIS, New Delhi India, 110002
49. Standards A (2016) ASTM A370/ASME SA-370 Standard test methods and definitions for mechanical testing of steel products 1. Am Soc Test Mater. https://doi.org/10.1520/A0370-16
50. Indian Standards, IS 456 (2000) Plain and reinforced concrete - code of practice, bureau of Indian standard, BIS, New Delhi India 110002
51. Indian Standards, IS 10262 (2019): Concrete mix proportioning-guidelines (second revision), bureau of Indian standards, BIS, New Delhi, India 110002, 2019. www.standardsbis.in
52. Saraswathy V, Muralidharan S, Thangavel K, Srinivasan S (2003) Influence of activated fly ash on corrosion-resistance and strength of concrete. Cem Concr Compos 25:673–680. https://doi.org/10.1016/S0958-9465(02)00068-9

53. Choi YS, Kim JG, Lee KM (2006) Corrosion behavior of steel bar embedded in fly ash concrete. Corros Sci 48:1733–1745. https://doi.org/10.1016/j.corsci.2005.05.019
54. Ha TH, Muralidharan S, Bae JH, Ha YC, Lee HG, Park KW, Kim DK (2007) Accelerated short-term techniques to evaluate the corrosion performance of steel in fly ash blended concrete. Build Environ 42:78–85. https://doi.org/10.1016/j.buildenv.2005.08.019
55. Chindaprasirt P, Rukzon S (2008) Strength, porosity and corrosion resistance of ternary blend Portland cement, rice husk ash and fly ash mortar. Constr Build Mater 22:1601–1606. https://doi.org/10.1016/j.conbuildmat.2007.06.010
56. Garces P, Andion LG, Zornoza E, Bonilla M, Paya J (2010) The effect of processed fly ashes on the durability and the corrosion of steel rebars embedded in cement-modified fly ash mortars. Cem Concr Compos 32:204–210. https://doi.org/10.1016/j.cemconcomp.2009.11.006
57. Boga AR, Topu LB (2012) Influence of fly ash on corrosion resistance and chloride ion permeability of concrete. Constr Build Mater 31:258–264. https://doi.org/10.1016/j.conbuildmat.2011.12.106
58. Kayali O, Sharfuddin Ahmed M (2013) Assessment of high volume replacement fly ash concrete-concept of performance index. Constr Build Mater 39:71–76. https://doi.org/10.1016/j.conbuildmat.2012.05.009
59. Azad AK, Ahmad S, Al-Gohi BHA (2010) Flexural strength of corroded reinforced concrete beams. Mag Concr Res 62:405–414. https://doi.org/10.1680/macr.2010.62.6.405
60. Yalciner H, Kumbasaroglu A, El-Sayed AK, Balkis AP, Dogru E, Turan AI, Karimi A, Kohistani R, Mermit MF, Bicer K (2020) Flexural strength of corroded reinforced concrete beams. ACI Struct J 117:29–41. https://doi.org/10.14359/51720195
61. Wang L, Zhang X, Zhang J, Ma Y, Xiang Y, Liu Y (2014) Effect of insufficient grouting and strand corrosion on flexural behavior of PC beams. Constr Build Mater 53:213–224. https://doi.org/10.1016/j.conbuildmat.2013.11.069
62. ASTM Standards, ASTM (2015) C876–15 Standard test method for corrosion potentials of uncoated reinforcing steel in concrete 1. https://doi.org/10.1520/C0876-15.
63. Sagüés AA, Kranc SC (1992) On the determination of polarization diagrams of reinforcing steel in concrete. CORROSION 48(8):624–633. https://doi.org/10.5006/1.3315982
64. Abdellatief M, Elrahman MA, Elgendy G, Bassioni G, Tahwia AM (2023) Response surface methodology-based modelling and optimization of sustainable UHPC containing ultrafine fly ash and metakaolin. Constr Build Mater 388:131696. https://doi.org/10.1016/j.conbuildmat.2023.131696
65. Abdellatief M, Al-Tam SM, Elemam WE, Alanazi H, Elgendy GM, Tahwia AM (2023) Development of ultra-high-performance concrete with low environmental impact integrated with metakaolin and industrial wastes. Case Stud Constr Mater 18:724. https://doi.org/10.1016/j.cscm.2022.e01724
66. Abd Ellatief M, Abadel AA, Federowicz K, Abd Elrahman M (2023) Mechanical properties, high temperature resistance and microstructure of eco-friendly ultra-high performance geopolymer concrete: Role of ceramic waste addition. Constr Build Mater 401:132677. https://doi.org/10.1016/j.conbuildmat.2023.132677
67. American Concrete Institute., ACI 546R-14: Guide to concrete repair, American Concrete Institute, 2014.
68. International Concrete Repair Institute, Guide for surface preparation for the repair of deteriorated concrete resulting from reinforcing steel corrosion [Guideline No. 310.1R–2008 (formerly No. 03730)], 2008. www.icri.org.
69. ACI Committee 440., American Concrete Institute., Guide for the design and construction of externally bonded FRP systems for strengthening concrete structures, American Concrete Institute, 2008
70. Indian Standards IS 516 (1959) Method of tests for strength of concrete, bureau of Indian standard, BIS, New Delhi India 110002
71. Bureau of Indian Standards (1999) IS 5816 (1999): method of test splitting tensile strength of concrete. New Delhi, India
72. Dhalape P, Sathe S, Dekhane C (2022) An experimental study on cement concrete with industrial fly ash and Phosphogypsum. Mater Today Proc. https://doi.org/10.1016/j.matpr.2022.11.365
73. Yalciner H, Kumbasaroglu A (2020) Experimental evaluation and modeling of corroded reinforced concrete columns. ACI Struct J 117:61–76. https://doi.org/10.14359/51721372
74. Celik A, Yalciner H, Kumbasaroglu A, Turan Aİ (2022) An experimental study on seismic performance levels of highly corroded reinforced concrete columns. Struct Concr 23:32–50. https://doi.org/10.1002/suco.202100065
75. ASTM standards, ASTM: G1–03 (2017) Standard practice for preparing, cleaning, and evaluating corrosion test specimens, American Society for Testing and Materials
76. Dong J, Zhao Y, Wang K, Jin W (2017) Crack propagation and flexural behaviour of RC beams under simultaneous sustained loading and steel corrosion. Constr Build Mater 151:208–219. https://doi.org/10.1016/j.conbuildmat.2017.05.193
77. ACI Committee 318, American Concrete Institute., International organization for standardization, building code requirements for structural concrete (ACI 318–08) and commentary, American Concrete Institute, 2008
78. American Concrete Institute, ACI 549.4R-13: Guide to design and construction of externally bonded fabric-reinforced cementitious matrix (FRCM) systems for repair and strengthening concrete and masonry structures, ACI Committee 549, 2013.